Dynamic Electrophoretic Assembly of Metal-Phenolic Films: Accelerated Formation and Cytocompatible Detachment

COMPASS
ENGINEERING LIFE GUIDED BY NATURE

This paper must be cited as: Yun, G., Youn, W., Lee, H., Han, S. Y., Oliveira, M. B., Cho, H., Caruso, F., Mano, J. F., & Choi, I. S. Dynamic Electrophoretic Assembly of Metal–Phenolic Films: Accelerated Formation and Cytocompatible Detachment. *32*(18), 7746-7753. *Chemistry of Materials* (2020). https://pubs.acs.org/doi/10.1021/acs.chemmater.0c02171

Dynamic Electrophoretic Assembly of Metal-Phenolic Films: Accelerated Formation and Cytocompatible Detachment

Gyeongwon Yun,[1] Wongu Youn,[1] Hojae Lee,[1] Sang Yeong Han,[1] Mariana B. Oliveira,[2] Hyeoncheol Cho,[1] Frank Caruso,[3] João F. Mano,[2] Insung S. Choi[1*]

[1] Center for Cell-Encapsulation Research, Department of Chemistry, KAIST, Daejeon 34141, Korea

[2] Department of Chemistry, CICECO—Aveiro Institute of Materials, University of Aveiro, 3810-193 Aveiro, Portugal

[3] ARC Centre of Excellence in Convergent Bio-Nano Science and Technology, and the Department of Chemical Engineering, The University of Melbourne, Parkville, Victoria 3010, Australia

Abstract

Kinetic and thermodynamic control of adhesion and cohesion is crucial in the dynamic manipulation of thin films. High adhesion enables material-independent film formation but contradictorily makes it difficult to detach the films and fabricate free-standing films under mild conditions. In this work, we developed an electrophoresis-based method, called dynamic electrophoretic assembly (dEPA), for dynamically and locally regulating the cohesive and adhesive processes of metal-phenolic materials. Locally concentrated cohesive process in the dEPA increases the film growth rate by two- or even three-orders of magnitude in the continuous fashion, and, more importantly, the simple current switching weakens only film adhesiveness and yields durable free-standing films under cytocompatible conditions. Various functional entities, including living cells, were incorporated into the films. Cytocompatibilit of the materials and processes in dEPA led to the fabrication of free-standing cell sheets.

Recent years have witnessed the unforeseen exploitation of the adhesion-cohesion rivalry[1] for material-independent coating and film formation, because the competition between cohesive molecule-molecule and adhesive molecule-substrate interactions determines whether the molecules coalesce or spread out over the surface.[2] In the coating process, adhesion wins in first-layer formation, and cohesion does in flocculation, precipitation, and gelation.[3] Nonspecific adhesive species, generated in situ in the solution phase, are also cohesive, granting but simultaneously interfering with the film growth, exemplified by polydopamine (PD)-[4] and metal-phenolic network (MPN)-based methods.[5] Their formation near to or at the substrate surface should not be excluded, but the fast termination in film growth suggests the predominant or uneven generation in the solution phase. High adhesion, enabling material-independent coating, does not allow for easy film detachment or delamination.[6] Weakened adhesiveness is coupled with weakened cohesiveness, leading to film degradation, not detachment, in the bulk process.[7] In this respect, kinetic and thermodynamic control of adhesive and cohesive processes is highly demanding to dynamically regulate the characteristics of the films being formed and detached. Recent examples include the in-situ oxidation of Fe^{2+} to Fe^{3+}, localized in the reaction space, which directs the localized cohesive interactions—ensuring the continuous film growth—as well as the adhesion-derived first-layer formation.[8] We also reported that relatively stable (i.e., less cohesive) metal-phenolic species, called metal**-**phenolic sol (MPS), led to the continuous film growth.[9]

Free-standing thin films and membranes have been fabricated for diversified applications in the materials sector.[10] Cytocompatibility of free-standing films is highly demanded in biomaterials,[11] biomembranes for organ-on-a-chip devices,[12] scaffolds for tissue

engineering,[13] and drug delivery.[14] For production of cytocompatible free-standing films, the layer-by-layer (LbL) technique has mainly been employed, but the reported process is time-consuming and requires nearly hundreds of LbL depositions.[15] In addition, LbL-film detachment is not compatible with bioentities, because it relies on the film drying in the air. The MPN film would be an alternative for the fabrication of cytocompable free-standing films, but the reported process uses organic solvents for film detachment, not applicable to bio-related fields, such as cell sheet engineering. In this work, we propose electrophoresis as a simple but advanced tool for dynamically regulating the cohesive and adhesive phenomena in the MPN-based, material-independent film formation. Specifically, the electrophoretic movement and localization of the MPS lead to the 10-to-350 fold acceleration in the continuous film growth, and film detachment is achieved with ease under cytocompatible conditions by simply switching the electrical potential, from positive to negative, at an electrode. Our strategy of dynamic electrophoretic assembly (dEPA) fabricates free-standing MPN films with arbitrary shapes and also with the combination of different metal ions, phenolic molecules, and functional entities.

The dEPA setup is composed of two indium tin oxide-coated glasses (ITO glasses), connected to an AA battery, in the Fe^{3+}-tannic acid (TA) MPS (**Figure 1**). In the setup, the MPS acted as both self-assembling block for the MPN film and conductive medium with the battery as a power source. The Fe^{3+}-TA MPS was prepared by mixing a TA solution (40 mg mL^{-1} in deionized (DI) water) with an equal volume of the $FeCl_3 \cdot 6H_2O$ solution (10 mg mL^{-1} in DI water), as described previously.[9] It was apparent to the naked eyes, upon the battery connection to the circuit, that only anodic (i.e., positively charged) ITO glass turned dark (bluish black), indicating the

formation of Fe^{3+}-TA MPN films from negatively charged MPS (**Figure 2a**; Figure S1, Supporting Information).

The electrophoretic movement in the dEPA system accelerated the cohesive process (i.e., attractive interactions) of the MPS locally at or near to the anodic electrode (Figure 2b,c).[16] The film-growth rate was calculated to be 46.7 nm h^{-1} for Fe^{3+}-TA MPS, which was about 7.5-fold higher than that for the conventional MPS system (6.2 nm h^{-1}),[9a] where the films are assembled in the absence of electrophoretic regulation. The Fe^{3+}-TA MPN film with a thickness of 560 nm was formed in 12 h of the dEPA regulation, whereas 89 h was required to make the film without electrophoretic control.[9] The rate enhancement was also observed with other metal ions and ligands, such as Ga^{3+}, In^{3+}, Tb^{3+}, gallic acid (GA), pyrogallol (PG), and pyrocatechol (PC) (Figure 2d,e; Figure S2, Supporting Information): astonishingly, the growth rates for Tb^{3+}-TA and Fe^{3+}-PC films increased by 350 and 100 times, respectively. In addition to the rate enhancement, the general utility of the dEPA system enabled the modularity control for the formation of multiple-metal MPN films, which was demonstrated by the formation of Fe^{3+}/Ga^{3+}/In^{3+}-TA multiple-metal films (Figure S3, Supporting Information). The Fe^{3+}-TA MPN films, as a representative, were characterized by scanning electron microscopy (SEM), UV-visible spectroscopy, and X-ray photoelectron spectroscopy (XPS), all confirming the successful film formation (Figures S4-S6, Supporting Information). The characterization also indicated that the dEPA process did not alter the chemical characteristics of the MPN film. The UV-visible absorption spectrum showed the ligand-to-metal charge-transfer (LMCT) band of the Fe^{3+}-TA complex at 565 nm (Figure S5, Supporting Information). The estimated area ratio of C=O, C-O, and C-C peaks in the C 1s XPS spectrum (33:85:100) was similar to that for the Fe^{3+}-TA film

without electrophoretic control (Figure S6, Supporting Information).[9a] The film was also degraded rapidly in the 1 M HCl solution (Figure S7, Supporting Information).[5]

Functional entities (e.g., enzymes, particles, and microorganisms) in the MPN films were embedded by the dEPA strategy that simply used the electrophoretic movement. As a proof-of-demonstration, an enzyme, β-galactosidase (β-Gal), was dissolved in the MPS, and the electrophoretic MPN assembly was performed for 24 h (Figure S8, Supporting Information). The 2,2-azinobis-(3-ethylbenzothiazoline-6-sulfonate) (ABTS) assay of the β-Gal-embedded Fe^{3+}-TA film, showing the strong absorption at 417 and 730 nm (Figure S8, Supporting Information), clearly indicated that β-Gal was not only well-embedded in the film but also enzymatically active. The versatility of our dEPA strategy was further confirmed with diverse functional materials, such as inorganic materials, polymers, and microorganisms. Spherically shaped iron nanoparticles (35-45 nm), SiO_2 nanoparticles (500 nm), polystyrene microparticles (3.2 μm), and even yeast cells (3-4 μm) were successfully incorporated into the Fe^{3+}-TA thin films, regardless of size and type (Figure S8, Supporting Information). Taken together, the dEPA-driven, localized cohesive process not only led to the extremely accelerated film growth but also had great potential in the component modularity.

The dEPA system weakened the adhesiveness of the MPN films, without disturbing the cohesion, by simply switching the potential from positive to negative, leading to film detachment under mild conditions. The XPS analysis indicated that the oxidation state of Fe ions (i.e., Fe^{3+}) and area ratio of C=O, C-O, and C-C bonds (i.e., 35:83:100) were unchanged after formation of

free-standing films (Figure S9, Supporting Information). The free-standing films that are adjustable in shape or pattern would be valuable platforms in a wide range of fields including biomedical and materials science,[17] and the shape controllability was demonstrated by the dEPA system. We used a polypropylene (PP) mask to make certain area of the electrode exposed to the MPS, and formed the free-standing films with various shapes including symbols and letters (**Figure 3a,b**; Figure S10, Supporting Information). The results also indicated that the localized electrostatic repulsion between the MPN film and the cathode played a crucial role in the peeling-off of the MPN films from the electrode. The free-standingfilm formed was found to be durable: while maintaining the original shape in an aqueous solution (pH 7) for more than six months, the film could be folded and unfolded many times, like paper origami (Figure 3c,d). The film detachment was general, confirmed by the free-standing-film formation of the Fe^{3+}/Ga^{3+}/In^{3+}-TA system and β-Gal-embedded Fe^{3+}-TA system (Figure 3e,f), which would enable versatile applications of the functional free-standing films.

It has been a challenging task in the biomaterials field to fabricate cytocompatible free-standing membranes and films with controlled porosity. For example, the free-standing membrane could act as a culture platform in microfluidic devices while permitting the penetration of small molecules, such as drug candidates or stimulants, from the medium.[18] Key requirements of free-standing films in this direction include that the free-standing film itself should be cytocompatible and/or so be the free-standing -film-forming process. In this respect, we thought that the dEPA would lead to the formation of free-standing cell sheets without any compromise in cell viability (**Figure 4a**). Before free-standing-film formation, we verified the

cytocompatibility of Fe^{3+}-TA MPN films with various cell types, such as NIH 3T3 fibroblast, HeLa, and HaCaT cells. An efficient adhesion and uniform distribution of fibroblast cells were observed after two days in culture (Figure 4b,c). The co-culture of three cell lines was made on the Fe^{3+}-TA film (Figure 4d), additionally indicating that the MPN film provided the cytocompatible surface environment to the cells. The current switching formed the free-standing cell sheets (Figure 4e), which were bent slightly due to cellular cohesion[19] but retained the 2D sheet morphology in the solution (Figure 4f). Of importance was the observation that the dEPA-driven film detachment did not affect the cell viability, proving that the electrophoretic regulation was the extremely cytocompatible process. We envisioned that the dEPA-based controls over film characteristics such as chemical compositions and mechanical stiffness, coupled with permselectivity of the MPN films[5,8d,9a,20] would advance cell-sheet engineering and related fields. For example, the bendability of the MPN film allowed for the fabrication of cylindrical cellular construct without any loss of cell viability (Figure 4g). We envision that more complex films could be produced by sequentially depositing different components along the time, producing stratified structures with controlled composition.

In summary, we demonstrated the electrophoretic approach to dynamically and locally regulate the adhesion and cohesion of metal-phenolic species, enabling cytocompatible fabrication of the free-standing films even with living cells. In addition to the cytocompatibility, our strategy has several advantages over the conventional methods: It forms the MPN films continuously, and the film growth is extremely fast; It could incorporate functional entities into the MPN film, regardless of their size or type, simply by mixing them with the MPS; It would be applied to any conducting materials, as an electrode, for film formation. For example, an electrode of the

microelectrode array was selectively activated and coated with the MPN for multiplexed applications. The process is controlled in a reversible fashion; it is scalable in size and shape, and requires low energy consumption, permitting the industry-level manipulation, because the dynamic regulation is based on the electrostatics at the interface between the MPN film and the substrate; the dEPA strategy is not limited to MPN films and can be applied to various free-standing-film formation with tunable thickness. We believe that the efficiency, versatility, and cytocompatibility of the dEPA method would provide new vistas on the fields of biomedical engineering and bioMEMs, such as tissue engineering, molecular diagnostics, and implantable microdevices.

Supporting Information

Supporting information is available from the Wiley Online Library or from the author.

Acknowledgements

This work was supported by the Basic Science Research Program through the National Research Foundation of Korea (NRF) funded by the Ministry of Science, ICT & Future Planning (MSIP2012R1A3A2026403), and the European Research Council grant agreement ERC-2014-ADG-669858 (ATLAS). This work was developed within the scope of the project CICECO-Aveiro Institute of Materials, UIDB/50011/2020 & UIDP/50011/2020, financed by national funds through the FCT/MEC and when appropriate co-financed by FEDER under the PT2020 Partnership Agreement. Part of this research was conducted and funded by the Australian Research Council (ARC) Centre of Excellence in Convergent Bio-Nano Science and Technology (Project No. CE140100036).

Conflict of Interest

The authors declare no conflict of interest.

Keywords

electrophoresis, free-standing films, material-independent coating, metal-phenolic network, thin films

References

[1] R. C. Remsing, *Proc. Natl. Acad. Sci. USA* **2019**, *116*, 23874.

[2] a) D. Y. Ryu, K. Shin, E. Drockenmuller, C. J. Hawker, T. P. Russell, *Science* **2005**, *308*, 236; b) J. J. Richardson, M. Björnmalm, F. Caruso, *Science* **2015**, *348*, aaa2491; c) H. Ejima, J. J. Richardson, F. Caruso, *Nano Today* **2017**, *12*, 136; d) H. A. Lee, Y. Ma, F. Zhou, S. Hong, H. Lee, *Acc. Chem. Res.* **2019**, *52*, 704.

[3] a) J. Guo, J. J. Richardson, Q. A. Besford, A. J. Christofferson, Y. Dai, C. W. Ong, B. L. Tardy, K. Liang, G. H. Choi, J. Cui, P. J. Yoo, I. Yarovsky, F. Caruso, *Langmuir* **2017**, *33*, 10616; b) T. Park, W. I. Kim, B. J. Kim, H. Lee, I. S. Choi, J. H. Park, W. K. Cho, *Langmuir* **2018**, *34*, 12318; c) S. Hong, Y. Wang, S. Y. Park, H. Lee, *Sci. Adv.* **2018**, *4*, eaat7457.

[4] H. Lee, S. M. Dellatore, W. M. Miller, P. B. Messersmith, *Science* **2007**, *318*, 426.

[5] H. Ejima, J. J. Richardson, K. Liang, J. P. Best, M. P. van Koeverden, G. K. Such, J. Cui, F. Caruso, *Science* **2013**, *341*, 154.

[6] a) P. G. de Gennes, *Rev. Mod. Phys.* **1985**, 57, 827; b) J. S. Rowlinson, B. Widom, *Molecular Theory of Capillarity*, Dover Publications, New York, USA **2002**.

[7] a) H. Nakanishi, M. E. Fisher, *Phys. Rev. Lett.* **1982**, *49*, 1565; b) M. E. Fisher, *J. Stat. Phys.* **1984**, 34, 667; c) J. H. Park, K. Kim, J. Lee, J. Y. Choi, D. Hong, S. H. Yang, F. Caruso, Y. Lee, I. S. Choi, *Angew. Chem. Int. Ed.* **2014**, *53*, 12420; d) J. Lee, H. Cho, J. Choi, D. Kim, D. Hong, J. H. Park, S. H. Yang, I. S. Choi, *Nanoscale* **2015**, *7*, 18918; e) C. Park, B. J. Yang, K. B. Jeong, C. B. Kim, S. Lee, B.-C. Ku, *Angew. Chem. Int. Ed.* **2017**, *56*, 5485.

[8] a) H. Lee, W. I. Kim, W. Youn, T. Park, S. Lee, T.-S. Kim, J. F. Mano, I. S. Choi, *Adv. Mater.* **2018**, *30*, 1805091; b) B. J. Kim, J. K. Lee, I. S. Choi, *Chem. Commun.* **2019**, *55*, 2142; c) S. Y. Han, S.-P. Hong, E. K. Kang, B. J. Kim, H. Lee, W. I. Kim, I. S. Choi, *Cosmetics* **2019**, *6*, 23; d) Q.-Z. Zhong, S. Li, J. Chen, K. Xie, S. Pan, J. J. Richardson, F. Caruso, *Angew. Chem. Int. Ed.* **2019**, *58*, 12563.

[9] a) G. Yun, Q. A. Besford, S. T. Johnston, J. J. Richardson, S. Pan, M. Biviano, F. Caruso, *Chem. Mater.* **2018**, *30*, 5750; b) G. Yun, J. J. Richardson, M. Biviano, F. Caruso, *ACS Appl. Mater. Interfaces* **2019**, *11*, 6404; c) G. Yun, J. J. Richardson, M. Capelli, Y. Hu, Q. A. Besford, A. C. G. Weiss, H. Lee, I. S. Choi, B. C. Gibson, P. Reineck, F. Caruso, *Adv. Funct. Mater.* **2020**, *30*, 1905805.

[10] a)) R. Qin, Y. Liu, F. Tao, C. Li, W. Cao, P. Yang, *Adv. Mater.* **2019**, *31*, 1803377; b) J. Liu, F. Yang, L. Cao, B. Li, K. Yuan, S. Lei, W. Hu, *Adv. Mater.* **2019**, *31*, 1902264; c) T. Zhang, H. Qi, Z. Liao, Y. D. Horev, L. A. Panes-Ruiz, P. St. Petkov, Z. Zhang, R. Shivhare, P. Zhang, K. Liu, V. Bezugly, S. Liu, Z. Zheng, S. Mannsfeld, T. Heine, G. Cuniberti, H. Haick, E. Zschech, U. Kaiser, R. Dong, X. Feng, *Nat. Commun.* **2019**, *10*, 4225.

[11] X. Zhang, C. Gong, O. U. Akakuru, Z. Su, A. Wu, G. Wei, *Chem. Soc. Rev.* **2019**, *48*, 5564.

[12] a) D. Huh, B. D. Matthews, A. Mammoto, M. Montoya-Zavala, H. Y. Hsin, D. E. Ingber, *Science* **2010**, *328*, 1662; b) H. Liu, Y. Wang, K. Cui, Y. Guo, X. Zhang, J. Qin, *Adv. Mater.* **2019**, *31*, 1902042.

[13] a) S.-H. Kim, H. R. Lee, S. J. Yu, M.-E. Han, D. Y. Lee, S. Y. Kim, H.-J. Ahn, M.-J. Han, T.-I. Lee, T.-S. Kim, S. K. Kwon, S. G. Im, N. S. Hwang, *Proc. Natl. Acad. Sci. U.S.A*

2015, *112*, 15426; b) K. Y. Morgan, D. Sklaviadis, Z. L. Tochka, K. M. Fischer, K. Hearon, T. D. Morgan, R. Langer, L. E. Freed, *Adv. Funct. Mater.* **2016**, *26*, 5873.

[14] a) Rui. R. Costa, M. Alatorre-Meda, J. F. Man, *Biotechnol. Adv.* **2015**, *33*, 1310; b) A. K. Yetisen, J. L. Martinez-Hurtado, B. Ünal, A. Khademhosseini, H. Butt, *Adv. Mater.* **2018**, *30*, 1706910.

[15] a) A. L. Larkin, R. M. Davis, P. Rajagopalan, *Biomacromolecules* **2010**, *11*, 2788; b) S. G. Caridade, C. Monge, F. Gilde, T. Boudou. J. F. Mano, *Biomacromolecules* **2013**, *14*, 1653; c) J. M. Silva, A. R. C. Duarte, S. G. Caridade, C. Picart, R. L. Reis, J. F. Mano, *Biomacromolecules* **2014**, *15*, 3817; d) T. D. Gomes, S. G. Caridade, M. P. Sousa, S. Azevedo, M. Y. Kandur, E. T. Öner, N. M. Alves, J. F. Mano, *Acta Biomater.* **2018**, *69*, 183.

[16] a) J. J. Richardson, H. Ejima, S. L. Lörcher, K. Liang, P. Senn, J. Cui, F. Caruso, *Angew. Chem. Int. Ed.* **2013**, *52*, 6455; b) G. Rydzek, Q. Ji, M. Li, P. Schaaf, J. P. Hill, F. Boulmedais, K. Ariga, *Nano Today* **2015**, *10*, 138.

[17] a) W. Gao, N. Singh, L. Song, Z. Liu, A. L. M. Reddy, L. Ci, R. Vajtai, Q. Zhang, B. Wei, P. M. Ajayan, *Nat. Nanotechnol.* **2011**, *6*, 496; b) D. Han, Y. Park, H. Kim, J. B. Lee, *Nat. Commun.* **2014**, *5*, 4367; c) R. Feiner, L. Engel, S. Fleischer, M. Malki, I. Gal, A. Shapira, Y. Shacham-Diamand, T. Dvir, *Nat. Mater.* **2016**, *15*, 679; d) J.-O. Kim, K.-I. Min, H. Noh, D.-H. Kim, S.-Y. Park, D.-P. Kim, *Angew. Chem. Int. Ed.* **2016**, *55*, 7116; e) J. Shin, S. Choi, J. H. Kim, J. H. Cho, Y. Jin, S. Kim, S. Min, S. K. Kim, D. Choi, S.-W. Cho, *Adv. Funct. Mater.* **2019**, *29*, 1903863.

[18] a) A. Cobo , R. Sheybani , E. Meng, *Adv. Healthcare Mater.* **2015**, *4*, 969; b) C. Hannesschlaeger, A. Horner, P. Pohl, *Chem. Rev.* **2019**, *119*, 5922.

[19] L. Shapiro, A. M. Fannon, P. D. Kwong, A. Thompson, M. S. Lehmann, G. Grübel, J.-F. Legrand, J. Als-Nielsen, D. R. Colman, W. A. Hendrickson, *Nature* **1995**, *374*, 327.

[20] J. H. Park, S. Choi, H. C. Moon, H. Seo, J. Y. Kim, S.-P. Hong, B. S. Lee, E. Kang, J. Lee, D. H. Ryu, I. S. Choi, *Sci. Rep.* **2017**, *7*, 6980.

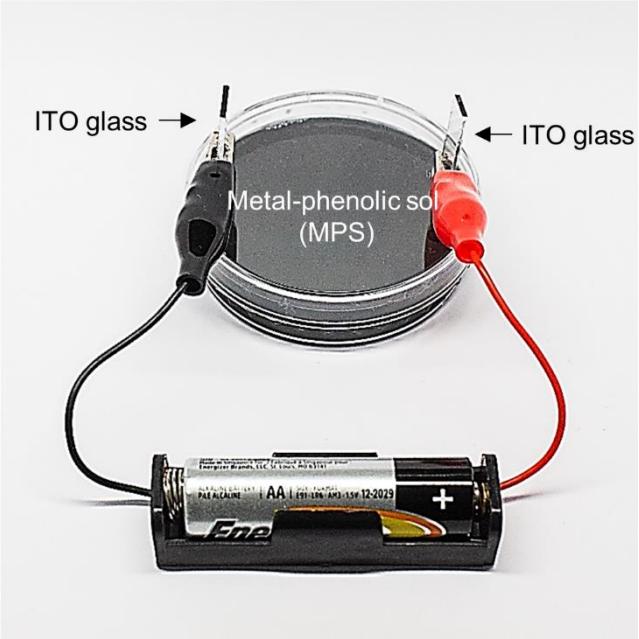

Figure 1. A digital photograph of the dEPA setup, composed of two ITO glasses, connected to an AA battery, in the MPS.

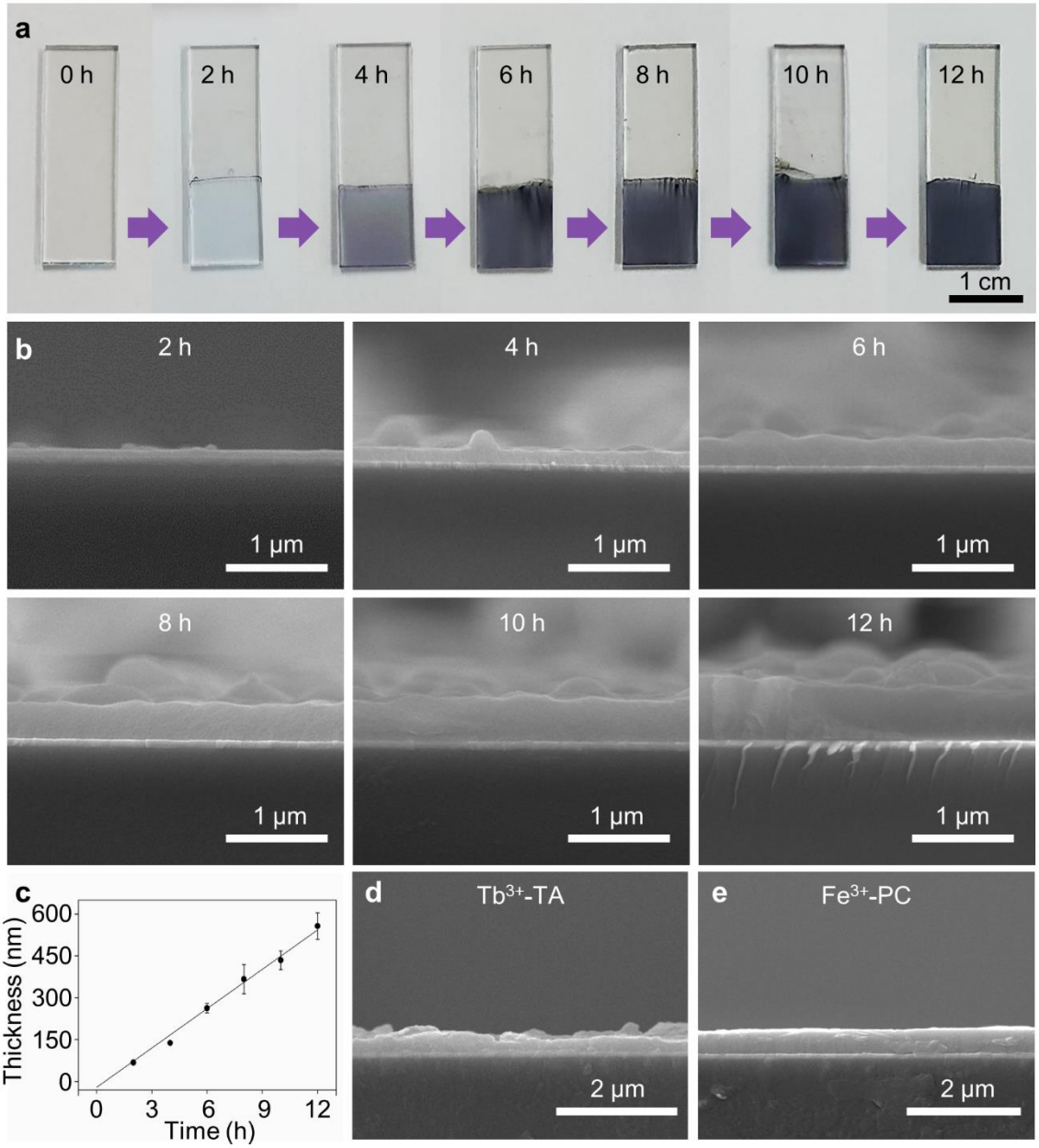

Figure 2. Characterization of the MPN films formed by dEPA. (a) Digital photographs of anodic ITO glasses at different dEPA reaction-times with Fe^{3+}-TA MPS. (b) Cross-sectional SEM images of Fe^{3+}-TA films at different dEPA reaction-times. (c) A graph of Fe^{3+}-TA-film thickness versus dEPA reaction-time. (d and e) Cross-sectional SEM images of Tb^{3+}-TA and Fe^{3+}-PC films after 14 h of dEPA.

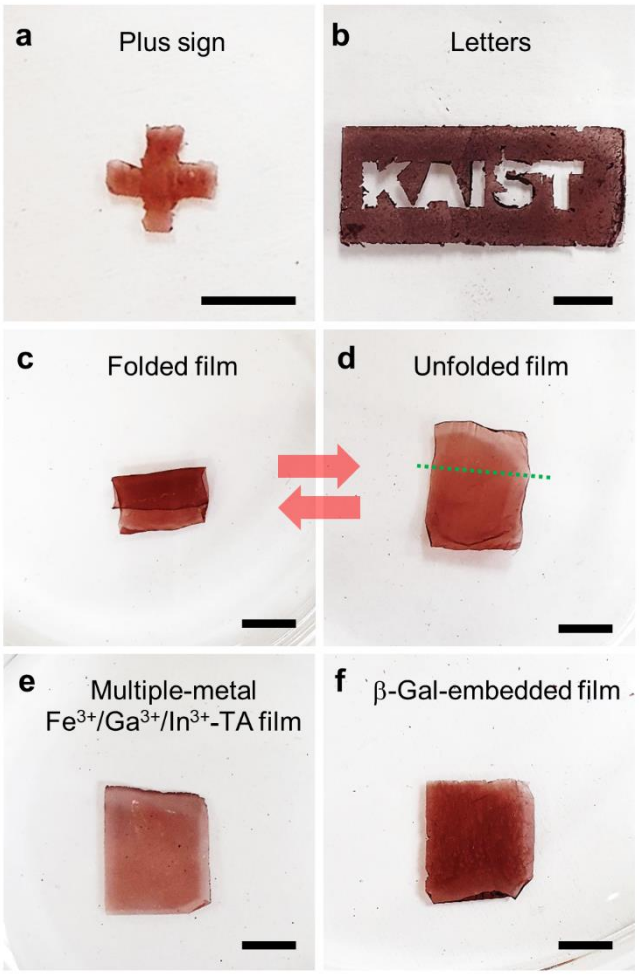

Figure 3. Fabrication and manipulation of free-standing films. (a and b) Digital photographs of shape-controlled, free-standing Fe^{3+}-TA films: (a) plus sign and (b) letters. (c and d) the folded and unfolded Fe^{3+}-TA films. (e) Free-standing multiple-metal $Fe^{3+}/Ga^{3+}/In^{3+}$-TA film. (f) β-Gal-embedded, free-standing Fe^{3+}-TA film. Scale bar: 0.5 cm.

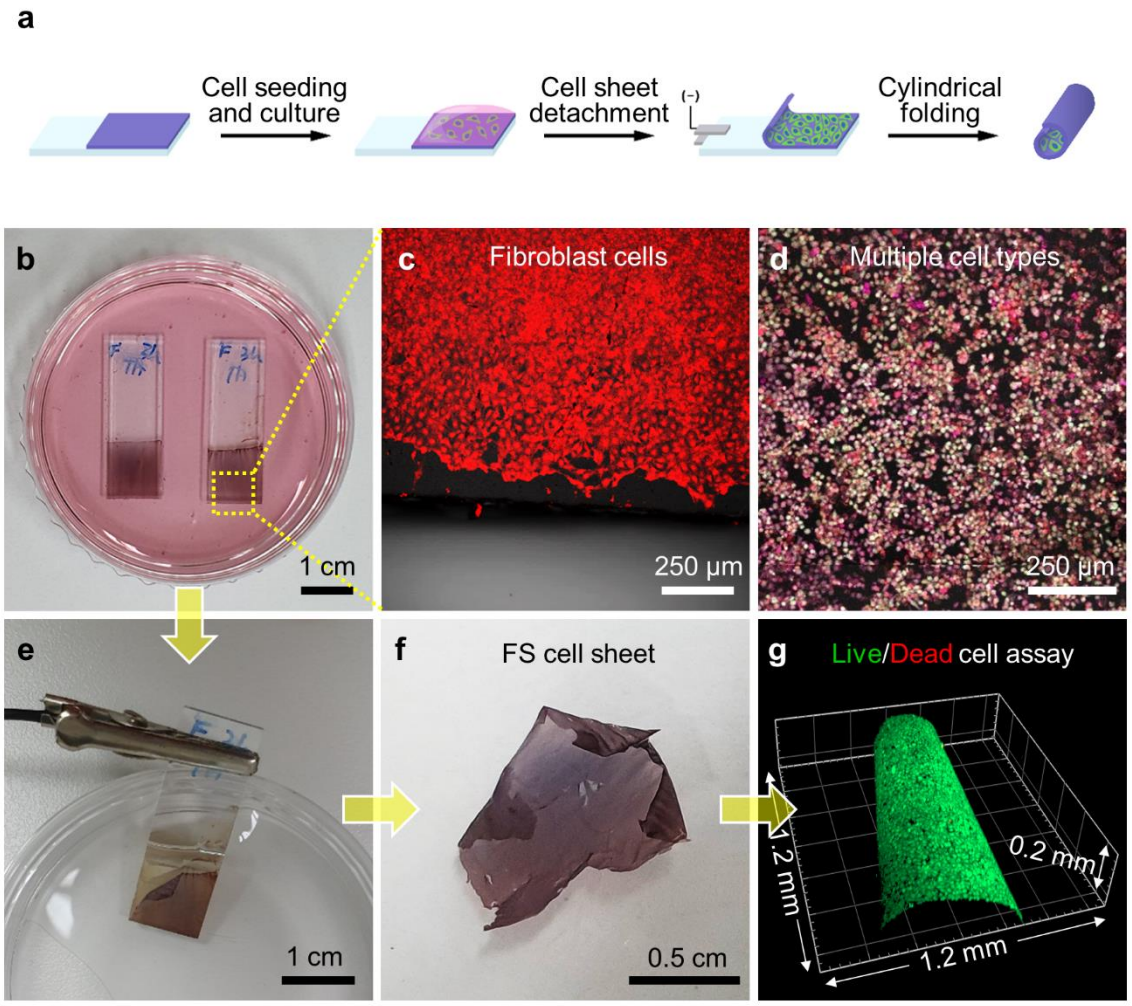

Figure 4. (a) Schematic for fabrication of free-standing cell sheets by dEPA. (b) A digital photograph of NIH 3T3 fibroblast cell sheets on the Fe^{3+}-TA film in the cell culture medium before detachment. (c and d) Confocal laser-scanning microscopy (CLSM) images of (c) fibroblast cells and (d) multiple cell types (NIH 3T3, HeLa, and HaCaT) on the Fe^{3+}-TA films. Red: NIH 3T3 fibroblast; green; HeLa; violet: HaCaT. (e and f) Digital photographs of fabrication of the free-standing cell sheet. (g) A 3D-reconstructed CLSM image of the free-standing fibroblast cell sheet after cylindrical folding. Green: live; red: dead.